Accurate Brake Torque Estimation With Adaptive Uncertainty Compensation Using a Brake Force Distribution Characteristic

Kyoungseok Han, Seibum B. Choi, *Member, IEEE*, Jonghyup Lee, Dongyoon Hyun, and Jounghee Lee

***Abstract*—This paper presents an adaptive individual brake torque estimation method based on the characteristic of front-to-rear brake force distribution ratio. Most previous studies on tire force estimation have assumed that brake torques can be calculated out of brake pressure and given fixed brake gains. However, brake gains are proportional to brake pad friction coefficients, which are influenced significantly by operating or weather conditions. In this paper, it is assumed that the pad friction coefficients are the only uncertainties of the wheel dynamics model since they vary significantly according to the driving conditions. Furthermore, the vehicle specific brake force distribution is used to obtain the additional information. Thus, more practical aspects can be considered when calculating the brake torque. The developed algorithm is verified through simulations and experiments using a production vehicle, and it confirms that the estimation performance is improved significantly compared with that without uncertainty compensation.**

***Index Terms*—Adaptive observer, brake force distribution ratio, tire slip, uncertainty compensation.**

I. Introduction

In ORDER to secure the vehicle stability control performance and maneuverability, various types of chassis control systems [1]–[4] have been developed and researched over the past two decades. The most important aspect in these systems is that the individual tire force, which determines the vehicle's attitude and direction, should be controlled appropriately in real time [5], [6]. That is, regardless of how intelligent the upper level controller that determines the target vehicle states is, the actuators in the lower level controller should generate appropriate control input with suitable timing. For example, antilock braking system (ABS) [7] has been developed to prevent wheels from locking up through adjusting the wheel pressure and thus enabling the wheel speed to track the desired wheel speed.

With the individual wheel pressure exerted by the driver, the amount of braking force depends on the brake torque that is calculated from the effective disc radii, wheel cylinder pressure, brake piston effective area and pad friction coefficient. Among these parameters, all variables are measurable or constant except the pad friction coefficient. However, the pad friction coefficient can change due to pad wear or variations in the pad-to-disc temperature [8]. In particular, the road surface or weather condition which directly affects the pad surface condition is the primary contributing factor that determines the amount of real brake torque. For example, the pad friction coefficient varies by up to 50% according to the road surface or weather conditions and this can cause under-or over-estimation of the brake torque. Influenced by wet brake pads, the brake torque is significantly decreased if the vehicle is traveling on wet road surfaces.

However, most previous studies [9]–[15] have assumed a fixed pad friction coefficient without consideration of the variations in the external environment, and the control strategy is designed based on a simply calculated brake torque. As a result of using an inaccurate brake torque, the longitudinal tire force might be under- or over-estimated, which might cause vehicle instability. Thus, accurate brake torque estimation through uncertainty compensation is critical; this is the basis of this paper.

The ultimate goal of compensating the pad friction coefficient is to accurately estimate the brake torque through reflecting the pad surface conditions. Thereby, the estimation results can be used as the basis for developing an active chassis control system. For example, any chassis control systems can be significantly enhanced if the peak tire-road friction coefficient is given in real-time [11]–[15]. Since the friction is calculated from tire forces, accurate real-time brake torque information can facilitate to estimate the maximum friction coefficient. In addition, it is also important to keep track of the desired value of the brake torque generated by the lower level controller, without unacceptable errors. Therefore, the proposed brake torque estimator can be an indicator for verifying the performance of the lower level controller.

In previous research regarding tire force estimation, the wheel speed has been predominantly used as a feedback term in the

Manuscript received February 19, 2017; revised May 17, 2017; accepted June 19, 2017. Date of publication June 28, 2017; date of current version December 14, 2017. This work was supported in part by Hyundai Motor Company; in part by the National Research Foundation of Korea (NRF) funded by the Korean government (MSIP) under Grant 2017R1A2B4004116; in part by the Ministry of Science, ICT, and Future Planning (MSIP), South Korea, under the Information Technology Research Center support program supervised by the Institute for Information and Communications Technology Promotion under Grant IITP-2017-2012-0-00628; in part by the Ministry of Trade, Industry & Energy(MOTIE), Korea Institute for Advancement of Technology(KIAT) through the Encouragement Program for The Industries of Region; and by the BK21+ program through the NRF funded by the Ministry of Education of Korea. The review of this paper was coordinated by Dr. K. Yu. *(Corresponding author: Seibum B. Choi.)*

K. Han, S. B. Choi and J. Lee are with the KAIST, Daejeon 34141, Korea (e-mail: hks8804@kaist.ac.kr; sbchoi@kaist.ac.kr; sonic_92@kaist.ac.kr).

D. Hyun and Jounghee Lee are with the Hyundai Motors Group, Hwaseong-si 445-706, Korea (e-mail: dyhyun@hyundai.com; jhmail@hyundai.com).

Color versions of one or more of the figures in this paper are available online at http://ieeexplore.ieee.org.

Digital Object Identifier 10.1109/TVT.2017.2720846

observer, but the practical aspects regarding the variations of the brake torque due to the aforementioned reasons are excluded. That is, the model that currently uses unaffordable uncertainty and compensation with only the wheel speed is not sufficient.

Moreover, simulation-based validation [9]–[11] cannot reflect the external environments, such as temperature, pad surface condition, and pad wear level; thus, only the constant brake gain is used to reflect the reliable brake torque. Therefore, these studies should consider practical brake torques when the proposed algorithm is implemented in passenger vehicles.

Several studies have elaborated on the design of the tire force observer with passenger vehicle based validation [12]–[15], but the brake torque remains an assumed value and only the wheel speed measurements contribute to compensate the model uncertainties. This inaccuracy in the currently used models highlights the importance of real-time identification of brake torque.

Though most existing studies have been designed based on a simple brake torque through multiplying the constant brake gain and wheel pressure; there are a few exceptions that consider the variations in the brake torque [16], [17].

In [16], the brake gain is estimated recursively using the wheel speed and brake pressure. However, this method cannot reflect the difference in the brake gain at the front and rear wheels because it only depends on the vehicle deceleration at the center of gravity. That is, only the average brake gain for the individual wheels is obtained in that study, but the brake gains at each wheel differ significantly due to the weight shifting effect. The temperature at the pad-disc contact surface was considered in [17], and the assumption that the heat generation is entirely absorbed and dissipated through the disc was used. However, the characteristics of the wet pad conditions vary significantly regardless of the temperature at the pad-disc surface. That is, the temperature model that is proposed in [17] is not valid when the vehicle travels on wet road surfaces.

The research presented in this paper is distinguished from others because the brake force balancing characteristic is adopted for each wheel in order to reflect the different brake torques at the front and rear wheels. This research aligns with the fact that most brake systems in passenger vehicles are designed to have a front bias in order to prevent oversteer. That is, the front wheel brake torques are saturated first due to the larger brake torques than those of rear. The force distribution ratio between the front and rear wheels does not change regardless of the tire-road friction coefficient as long as brake control unit (BCU) is not modified. The distributed force is only affected by the driver's brake pedal travel.

Furthermore, a Lyapunov-based adaptation is adopted in order to identify the lumped model uncertainty. The sensor signals used in this research are only vehicle acceleration and wheel speeds, which are readily available in passenger vehicles [18].

The proposed estimator has been investigated by simulations and passenger vehicle-based experiments on various road surfaces, particularly wet conditions, in order to confirm the effectiveness of the developed method. The tire force estimation results exhibit superior performance compared with the results estimated using the nominal pad friction coefficient.

This paper is organized as follows. In order to facilitate the problem formulation, the model uncertainty in the wheel dynamic and brake torque distribution concept is introduced in Section II. The core contribution of this paper, i.e., exploiting the brake system characteristics, is presented in Section III. In Sections IV and V, the developed algorithm is verified by simulations and passenger vehicle-based experiments, and the paper is concluded in Section VI.

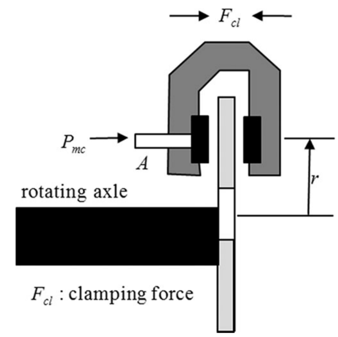

Fig. 1. Hydraulic brake system with a fixed caliper.

II. Problem Formulation

Based on the wheel dynamics, the longitudinal tire force can be identified and it is critical in designing the active chassis control system. The tire brake force is proportional to the amount of brake torque, which can be varied according to the pad conditions. The contributing factors that affect the pad conditions are as follows.

First, the temperature between the disc and pad surface can affect the brake torque. In general, the brake torque increases as the temperature at the disc-pad surface increases, but the amount of variation in the temperature is not significant. In [8], only a small amount of variation in the pad friction coefficient due to the temperature effect was observed. Therefore, it is not sufficient to initiate research on this subject.

Second, the pad characteristics are varied due to the changing pressure, deformation, and wear. However, it is not possible to observe these states in real time because the material property that influences these parameters is difficult to research due to its nonlinearity.

The most dominant factor that affects the pad surface condition is the level of wetness on the pad surface, which is influenced by the road surface conditions. In [8], the test results demonstrated that wet pad surfaces had half the amount of friction coefficient compared with dry pad surfaces.

A. Model Uncertainty in Wheel Dynamics

The wheel dynamics can be expressed as follows:

$$J_w \dot{\omega} = RF_x - T_b, \tag{1}$$

where J_w is the wheel rotational inertia, ω is the wheel angular velocity, R is the wheel effective radius, F_x is the tire longitudinal force, and T_b is the brake torque.

As depicted in Fig. 1, the brake torque consists of the following design parameters:

$$T_b = \mu_p \cdot A \cdot r \cdot P_{mc}, \tag{2}$$

TABLE I
SPECIFICATIONS OF THE HYDRAULIC BRAKE SYSTEM

Parameter	Quantity	Value
A_f	Wheel cylinder area at the front brake piston	28.84 cm^2
r_f	Effective radius of the front disc	130.9 mm
$\mu_{p,f}$	Nominal pad friction coefficient at the front brake pad	0.38
A_r	Wheel cylinder area at the rear brake piston	11.34 cm^2
r_r	Effective radius of the rear disc	124.0 mm
$\mu_{p,r}$	Nominal pad friction coefficient at the rear brake pad	0.38

where μ_p is the pad friction coefficient, A is the brake piston effective area, r is the brake disc effective radii and P_{mc} is the master cylinder pressure.

The nominal values of the parameters in Table I are the same as those of a commercially available medium sized sedan, which is used as the test vehicle in this paper.

For convenience, the constant parameters in (2) are considered together and the pad friction coefficient is divided into the nominal and unknown parts as follows:

$$T_b = (\mu_{p,n} + \xi) \cdot C \cdot P_{mc}, \tag{3}$$

where $\mu_{p,n}$ is the nominal pad friction coefficient, ξ is the unknown varying part in the pad friction coefficient and $C = A \cdot r$.

In (1), the model uncertainties such as the rolling resistance, aerodynamics, pad friction coefficient, and mismatch in effective tire radius are not explicitly considered, but these uncertainties can affect the (1).

However, it should be noted that the aim of this research is not to estimate the individual model uncertainties in (1), but rather to obtain the precise wheel dynamic model. Therefore, the strategy of all model uncertainties being assigned to the pad friction coefficient is proposed. The reason for adopting this approach is that inaccurate estimations for individual uncertainties can worsen the model. Furthermore, the factor that contributes to the model error cannot be easily distinguished even though individual identification is conducted.

The effect on the wheel dynamics due to the changing pad friction coefficient is considered to be more substantial than other factors. Therefore, the model used in this research that has a multiplicative uncertainty form [19] including all model uncertainties, is as follows:

$$J_w \dot{\omega} = \bar{F} R F_z - (\mu_{p,n} + \zeta) \cdot C \cdot P_{mc}, \tag{4}$$

where $\bar{F}$ is the current normalized tire force, F_z is the tire normal force, and ζ is the lumped model uncertainty.

In general, $\bar{F}$ varies according to the various kinds of parameters such as braking force, normal force and deceleration. Provided that accurate brake torque is given in (4), $\bar{F}$ can be easily obtained from the simple open-loop calculation. However, especially on a wet road surface condition, the brake torque during actual braking cannot be accurately provided. Therefore, $\bar{F}$ should be regarded as unknown varying parameter, and it is well known that maximum value of $\bar{F}$ is limited by the road surface type [12]–[16].

TABLE II
TEST VEHICLE SPECIFICATIONS

Parameters	Quantity	Values
M_v	Gross vehicle weight (2UP)	1744 kg
l_f	Distance between the front axle and center of gravity	1.1556 m
l_r	Distance between the rear axle and center of gravity	1.6494 m
l_w	Track width	1.55 m
h	Height of center of gravity	0.615 m
R	Effective tire radius	0.322 m
J_ω	Spin inertia for each wheel	0.7 kg $\cdot$ m^2

In this paper, a new strategy to identify $\bar{F}$ using the brake torque distribution ratio and the deceleration at the center of gravity is introduced.

B. Brake Force Distribution Strategy

It is generally accepted that the deceleration of a vehicle during braking is determined by the braking force as follows:

$$\frac{a_x}{g} = \frac{F_{xf} + F_{xr}}{M_v g}, \tag{5}$$

where a_x is the deceleration at the center of gravity, g is the gravitational constant, M_v is the total vehicle mass and F_{xf} and F_{xr} are the braking forces at the front and rear wheels, respectively.

Furthermore, a load transfer from the rear to the front axle occurs during braking. Therefore, the normal forces at the front and rear wheels that ignore the inclination of the road and the aerodynamics are expressed as follows:

$$F_{zf} = \frac{M_v g l_r - M_v a_x h}{l_f + l_r}, \tag{6}$$

$$F_{zr} = \frac{M_v g l_f + M_v a_x h}{l_f + l_r}, \tag{7}$$

where F_{zf} and F_{zr} are the tire normal force at the front and rear wheels, respectively, and the other parameters are described in Table II.

In addition, the braking forces of the front and rear wheels have a relationship with the normal forces, as follows:

$$\frac{F_{xf}}{F_{xr}} = \frac{\bar{F}_f F_{zf}}{\bar{F}_r F_{zr}} = \frac{\bar{F}_f \left[l_r - (a_x/g)h\right]}{\bar{F}_r \left[l_f + (a_x/g)h\right]}, \tag{8}$$

where $\bar{F}_f$ and $\bar{F}_r$ are the current normalized tire forces at the front and rear wheels, respectively.

As briefly stated above, the braking force should be proportional to the brake torque as follows [20],

$$\frac{T_{br}}{T_{bf}} = \frac{R_r F_{xr}}{R_f F_{xf}} \approx \frac{F_{xr}}{F_{xf}}. \tag{9}$$

where R_f and R_r are the effective radius of wheel at the front and rear wheels, and those values are assumed to be nearly the same.

Using this relationship, the brake torque curve on the front and rear wheels can be obtained from the following relations, as illustrated in Fig. 2 [20]:

$$T_{br} = \frac{\bar{F}_r \left[l_f + (a_x/g)h\right]}{\bar{F}_f \left[l_r - (a_x/g)h\right]} T_{bf}, \tag{10}$$

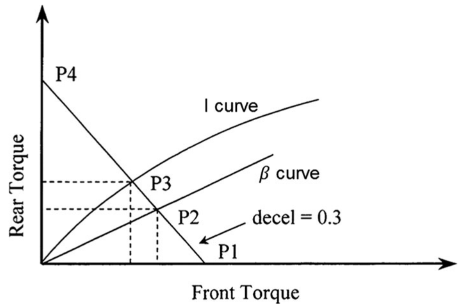

Fig. 2. Brake torque balancing strategy.

where T_{bf} and T_{br} are the brake torque at the front and rear wheels respectively

In vehicle design, the actual braking torques on the front and rear wheels are designed to have a fixed linear proportion using a hydraulic valve control or a fixed proportioning valve. Therefore, the brake torques are designed to be front biased such that the front brake torques are saturated first in order to prevent oversteer. As described in Table I, the parameters related to the front brake system have significantly larger values than those for the rear in order to generate a larger brake torque. Therefore, the brake torque distribution curve in Fig. 2 follows the β curve, and P2 is the torque distribution ratio when the vehicle is decelerating at 0.3 g.

The *I* curve in Fig. 2 is the ideal brake torque distribution curve where front and rear brake torques have the same value. However, these ideal torque distribution cannot be realized in the production vehicles due to the front biased torque distribution [20].

III. Proposed Algorithms

A. Algorithm Overview

Note that the two unknown parameters ($\bar{F}$ and ζ) that cannot be directly measured are included in (4), but only one equation is given. Mathematically, it is impossible to obtain the two parameters at the same time using only one equation.

Furthermore, it is difficult to use a different adaptation scheme [21] in this case due to the similar frequency range of the given inputs (F_z and P_{mc}) in (4). Therefore, additional information from other sources is required in order to obtain one unknown parameter. In this paper, a new strategy to simultaneously estimate the current normalized tire forces for the front and rear wheels ($\bar{F}_f$ and $\bar{F}_r$) is introduced.

It is generally assumed that the current normalized tire force at the front wheel has a larger value than that at the rear due to the front-biased fixed brake torque distribution ratio during braking. Also, the deceleration at the center of gravity has a relationship with the decelerations at each wheel.

The following equations can be induced if the aforementioned assumption is applied:

$$\bar{F}_f = \frac{a_x}{g} + f_1, \tag{11}$$

$$\bar{F}_r = \frac{a_x}{g} + f_2, \tag{12}$$

where f_1 and f_2 are the positive and negative values, respectively, and all parameters have dimensionless units.

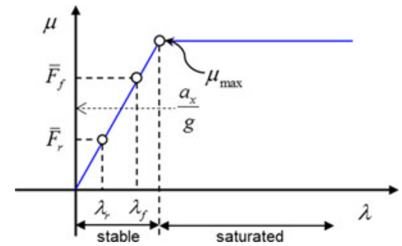

Fig. 3. Mu-slip curve.

Through monitoring the real-time deceleration of the vehicle, the a_x/g can be obtained, but unknown terms remain in (11) and (12). Therefore, the braking characteristics of most passenger vehicles are used to obtain f_1 and f_2. The detailed process to obtain these is discussed in the next section.

Also, the parameter adaptation is conducted in order to compensate the uncertainties in (4), and a more accurate wheel dynamic model is obtained.

B. Design of Normalized Force Curve

Fig. 3 describes the well-known relationship between the tire-road friction coefficient and tire slip [22], [23]. It depicts linearity until the vehicle reaches the peak friction point, and this region is defined as a stable area. However, the region that is marked as saturated provides different behavior of the vehicle because the tires lose their adhesion to the road surface due to the increased tire slip.

In this paper, it is assumed that the vehicle is not near the peak point in order to exclude the saturated region in this study because most braking conditions arise within the stable area. Also, it should be noted here that $\bar{F}_f$ and $\bar{F}_r$ are estimated in real-time since these values vary during braking, but estimation of maximum friction $\mu_{\max}$ is excluded from the scope of this study.

Note that the front tire slip has a significantly larger value than the rear for safety reasons, and both are proportional to their tire slips, as depicted in Fig. 3. Moreover, the vehicle deceleration is between these values as explained at the previous section. All values in Fig. 3 use the absolute value for the convenience.

Substituting (6) and (7) into (4), the wheel dynamics for the front and rear wheels can be expressed as follows:

$$J_w \dot{\omega}_f = \bar{F}_f R_f \left(\frac{M_v g l_r - M_v a_x h}{l_f + l_r} \right) - (\mu_{p,f} + \zeta_f) \cdot C_f \cdot P_{mc}, \tag{13}$$

$$J_w \dot{\omega}_r = \bar{F}_r R_r \left(\frac{M_v g l_f + M_v a_x h}{l_f + l_r} \right) - (\mu_{p,r} + \zeta_r) \cdot C_r \cdot P_{mc}. \tag{14}$$

The current normalized forces are functions of the tire slips, as follows:

$$\bar{F}_f = \frac{a_x}{g} + f_1 = f(\lambda_f), \tag{15}$$

$$\bar{F}_r = \frac{a_x}{g} + f_2 = f(\lambda_r). \tag{16}$$

Also, since the center of gravity of the vehicle has only one deceleration, the uncertainties, i.e., f_1 and f_2, have a specific relationship as follows.

The sum of the longitudinal forces can be expressed with the normal forces as follows,

$$\sum F_x = M_v a_x = F_z \frac{a_x}{g} = \bar{F}_f F_{zf} + \bar{F}_r F_{zr} \quad (17)$$

Substituting (15) and (16) to the (17), then the following relationship is derived.

$$F_z \frac{a_x}{g} = \left(\frac{a_x}{g} + f_1\right) F_{zf} + \left(\frac{a_x}{g} + f_2\right) F_{zr}$$
$$\rightarrow f_1 = -\frac{F_{zr}}{F_{zf}} f_2. \quad (18)$$

Based on (11) to (16), it is clear that the wheel dynamic during braking is a function of the deceleration and brake torque. The other parameters are constant, except $\bar{F}_{f,r}$ and $\zeta_{f,r}$ in (13) and (14). It must be noted that the brake torque distribution ratio between the front and rear wheels is determined regardless of the road surface or driver because it is a fixed value according to the vehicle design specifications and does not change before the BCU is modified. Using these characteristics, the novel method is presented next.

The tire slips for the front and rear wheels during braking are defined as follows:

$$\lambda_f = \frac{V - R\omega_f}{V}, \quad (19)$$

$$\lambda_r = \frac{V - R\omega_r}{V}, \quad (20)$$

where V is the absolute vehicle speed.

Combining (19) and (20), the following equation can be induced:

$$V = \frac{R\omega_f}{1 - \lambda_f} = \frac{R\omega_r}{1 - \lambda_r}. \quad (21)$$

Manipulating (21), a new parameter is proposed as follows:

$$\eta = \frac{1 - \lambda_r}{1 - \lambda_f} = \frac{\omega_r}{\omega_f}, \quad (22)$$

In general, it is clear that the tire slip is difficult to obtain when the vehicle begins to brake because the exerted brake force is transferred to all wheels. That is, the absolute vehicle speed cannot be measured.

However, an amount of slip ratio between the front and rear wheels can be inferred from the measured wheel speeds in (22). For example, η is larger than one during braking because λ_f is significantly larger than λ_r due to the brake torque distribution ratio and η increases as the amount of brake force increases.

Based on this principle, it can be assumed that the level of the braking intensity can be inferred from η. Thus, the new parameter, η, is proposed, and the key virtue of using η is that new information for use in (4) can be created from the η.

In order to confirm the proposed approach, a ramped brake pressure input was exerted by driver, as depicted in Fig. 4. In this process, a very wide range of tire slip was constructed with the ramped brake pressure input.

As depicted in Fig. 5, the current normalized forces at the front and rear wheels have different values due to the fixed front biased brake torque distribution ratio, and the front wheels have a significantly larger value than that of rear. Also, the deceleration

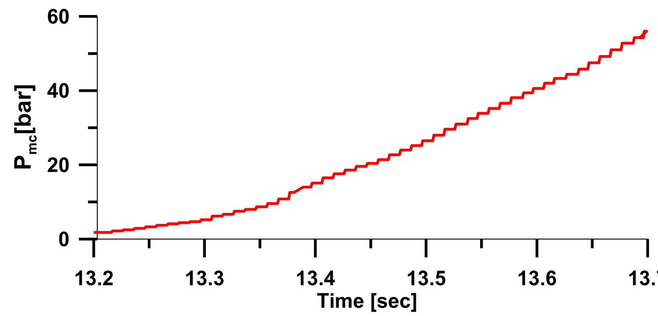

Fig. 4. Master cylinder pressure profile.

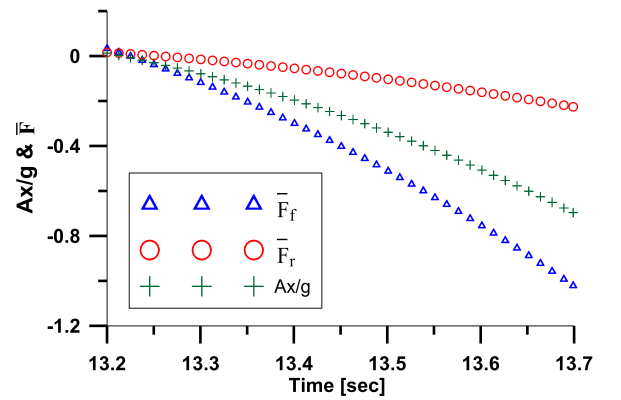

Fig. 5. Decelerations at each position: front wheel, rear wheel, and center of gravity.

at the center of gravity is in between the two normalized forces, and the values obtained are interpolated to create a clear lookup table. The normalized forces at each wheel are obtained from the wheel dynamics of (1) and normal force calculations of (6) and (7).

The reason for the normalized force at the front wheel being closer to the deceleration at the center of gravity than that at the rear is that the braking performance is primarily governed by the front wheel.

The amount of differences, i.e., f_1 and f_2, can be obtained based on Fig. 5, and a further step can be taken because the brake torque distribution ratio is a fixed value.

The current normalized forces at each wheel, i.e., $\bar{F}_f$ and $\bar{F}_r$, are proportional to their tire slips, but tire slips are difficult to be obtained directly. Therefore, the tire slip is inferred from the η.

Since the brake torque distribution ratio is only determined by the brake pedal travel, the η required to generate a specific deceleration does not change at the same road surface. For this reason, the road surface condition is immediately informed to the vehicle if the a_x and η is given in real-time.

Fig. 6 presents the relationship between $f_{1,2}$ and η at the wet asphalt. Based on this curve, the current normalized forces, i.e., $\bar{F}_f$ and $\bar{F}_r$, can be identified at the wet asphalt.

This induced curve can be applied to the passenger vehicle because the amount of f_1 and f_2 according to η is not changed due to the fixed brake torque distribution ratio at the BCU.

Since the introduced lookup table does not change unless the control strategy of the BCU is modified, a single well-made

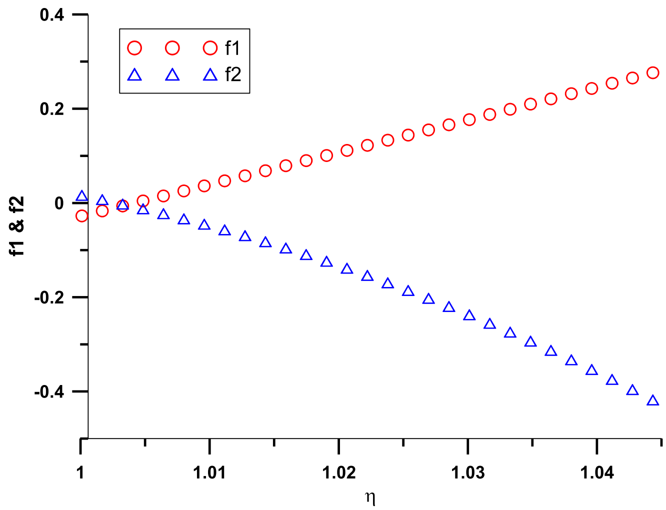

Fig. 6. Individual normalized force curve according to η.

experiment is sufficient to construct the lookup table before releasing the vehicle.

It is difficult to identify the tire slips at each wheel, but the integration information of the tire slips is available when the proposed parameter is used. Therefore, access to the information of each wheel is easier compared with other estimation methods.

C. Uncertainty Compensation in Wheel Dynamics

In this section, the uncertainty in the wheel dynamics is compensated using the adaptive scheme [21]. The new source from the individual normalized force curve in Fig. 6 enables (4) to be solved because ζ, which is imposed in the lumped model uncertainty, is the only unknown term.

For convenience, the derivation is only conducted for the front wheel because the same process is used for the rear wheel.

Based on the proposed approach, (4) can be separated into the known terms and the unknown terms as follows:

$$y = J_w \dot{\omega}_f - \left(\frac{a_x}{g} + f_1\right) R_f F_{zf} + \mu_{p,n} \cdot C_f \cdot P_{mc} = -\zeta_f \cdot C_f \cdot P_{mc} \tag{23}$$

Here, y is the output that can be measured from the readily available sensors and subscript f means front wheel, and ζ_f is the parametric uncertainty in pad friction coefficient and it should be adapted in real-time.

Consider the following:

$$y = \theta^* u(t), \tag{24}$$

where $\theta^* = \zeta_f$ and $u(t) = -C_f \cdot P_{mc}$.

Based on this, the adaptation laws can be established using the gradient method, as follows:

$$\dot{\hat{\theta}}^* = \gamma \varepsilon u(t), \tag{25}$$

where γ is a positive adaptation gain, $\hat{\bullet}$ is the estimated parameter, and $\epsilon = y - \hat{y}$.

Now, the stability of the designed adaptive law is analyzed.

The Lyapunov function is selected as follows:

$$V(\tilde{\theta}) = \frac{\varepsilon^2}{2\gamma}. \tag{26}$$

Differentiating the Lyapunov function with respect to time leads to

$$\dot{V}(\tilde{\theta}) = \frac{\varepsilon \dot{\varepsilon}}{\gamma} = \frac{\varepsilon(-\dot{\hat{y}})}{\gamma} = -\frac{\varepsilon(\dot{\hat{\theta}}^* u(t))}{\gamma} \tag{27}$$

If the established adaptive law is applied, then

$$\dot{V}(\tilde{\theta}) = -\frac{\varepsilon\left[\{\gamma \varepsilon u(t)\} u(t)\right]}{\gamma} = -\varepsilon^2 u^2(t) \le 0. \tag{28}$$

Through applying Barbalat's Lemma [24], it can be concluded that ε converges to zero as $t \to \infty$.

Fig. 7 shows that the overall block diagram of the proposed algorithm. The required signals are only the deceleration and wheel speeds, and these are readily available signals in the production vehicles.

IV. Simulation Studies

The effectiveness of the proposed algorithm was verified by simulation studies before production vehicle-based verification. The vehicle model and tire model used in the simulation are provided by CarSim software, which is a commercial vehicle dynamic solver package.

The nominal pad friction coefficient for front and rear wheels was set at 0.4, but uncertainty was intentionally imposed to verify the proposed algorithm. That is, nominal value for front pad friction coefficient was assumed to be 0.5, and the bigger uncertainty, i.e., 0.6, was imposed on the rear pad friction coefficient. However, the actual value was 0.4 which is the same for the both wheels. The ultimate goal of this simulation studies is to compensate model uncertainties in pad friction coefficients. Fig. 8 described the wheel speeds profile, and brake force was exerted at $t = 5$. Model uncertainties in pad friction coefficients were compensated as depicted in Fig. 9. Because the additional uncertainty for the front wheel was about 0.1, the proposed adaptation algorithm attempted to compensate for this uncertainty based on the front wheel dynamics. In addition, uncertainty in the rear wheel was also compensated well, although different model uncertainty, i.e., 0.2, was imposed in Fig. 9.

As a result of the uncertainty compensation, the brake torques in Figs. 10 and 11 much more consistent with the actual values, which were provided by CarSim software. However, the brake torques calculated from the uncompensated pad friction coefficient were different from the actual values, and it could cause instability of the vehicle dynamics. Also, the basis of this paper such that front brake torque have the larger value than that of rear is verified from Figs. 10 and 11.

V. Experimental Results

In order to verify the performance of the developed algorithm, experiments were conducted using a test vehicle. Fig. 12 is a photographs of the test vehicle and Table II provides the specifications of the test vehicle, which is identical to a commercially available vehicle. In addition, numerous test scenarios were

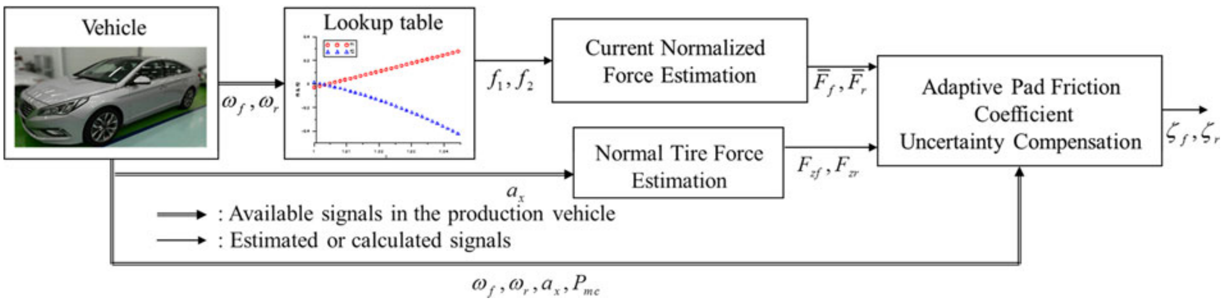

Fig. 7. Overall block diagram of the proposed algorithm.

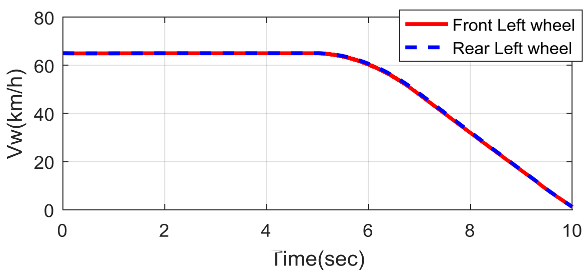

Fig. 8. Wheel speeds.

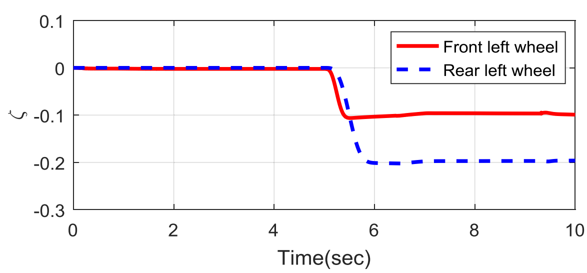

Fig. 9. Model uncertainties compensations.

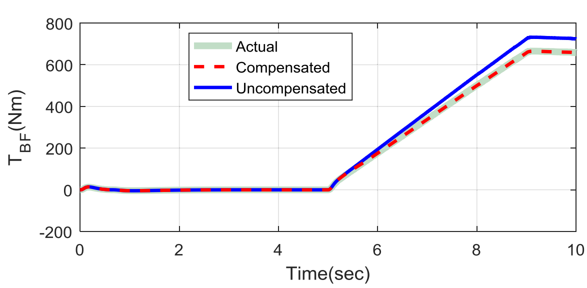

Fig. 10. Comparison of front left brake torques.

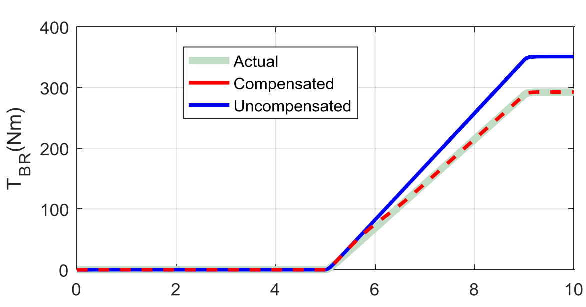

Fig. 11. Comparison of rear left brake torques.

Fig. 12. Test vehicle (medium sized sedan).

undertaken at the proving ground, which had various road surface conditions

A. Experimental Setup

The test vehicle was equipped with a VBox from Racelogic to report the vehicle absolute velocity in order to monitor each tire slip in real time. Other information about the vehicle states, e.g. wheel speeds and deceleration at the center of gravity, was obtained through a CAN BUS monitoring system. Furthermore, the proposed adaptive observer was operated with a 5 ms sampling time, and no computational burden was found.

The wet road surface condition was created by sprinkler systems that provided the rainy weather condition. Because only a limited area was affected by the sprinkler system, the test vehicle stayed on the wet surface by the sprinkler system for a sufficient time to change the pad surface condition. Considering practical concerns, the process performed was reasonable, since the pad friction condition was always influenced by the wet road surfaces or rain.

Also, the goal of this test is to estimate the variation in the pad surface friction coefficient.

B. Test Results

The effectiveness of the developed algorithms is verified on various road surfaces that include wet tile, basalt surface, and dry asphalt. The first experiment scenario that is depicted in Fig. 13 demonstrates the effectiveness of the estimator when the vehicle is traveling on dry asphalt with $\mu_{max} \approx 1.0$. The wheel speeds and deceleration were described in Fig. 13(a) and (b), and the current normalized forces for front and rear wheels are depicted

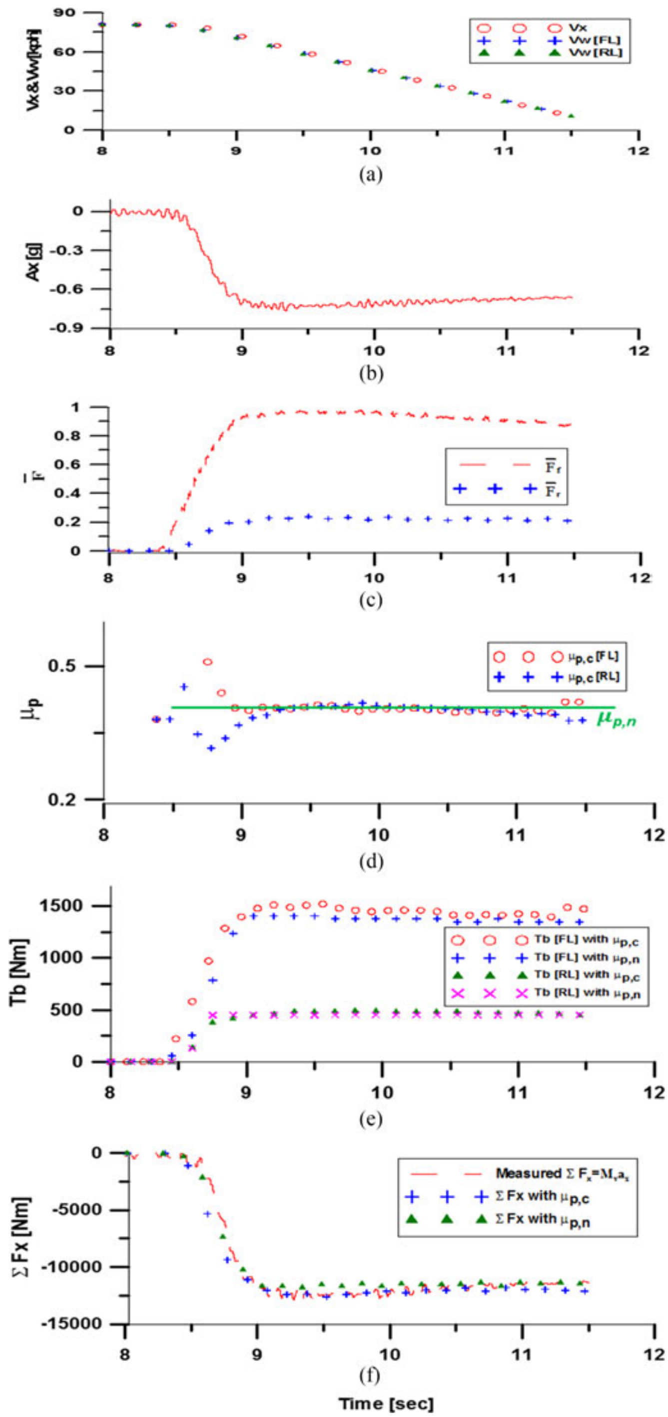

Fig. 13. Algorithm verification on a dry asphalt surface with $\mu_{\max} \approx 1.0$.

in Fig. 13(c). As expected, front normalized force had a larger value than that of rear due to the braking characteristic.

In addition, the very small model uncertainty was compensated as depicted in Fig. 13(d). The compensated pad friction coefficients were near the nominal pad friction, i.e., $\mu_{p,n} = 0.38$.

Consequently, Fig. 13(f) shows that the sum of the braking force with nominal pad friction coefficient ($\mu_{p,n}$) did not differ significantly to the braking force calculated with compensated pad friction coefficient ($\mu_{p,c}$). In the passenger vehicle test, it is a very expensive, technically difficult, and time-consuming task to attach a tire force transducer to the wheels that measures the real-time individual tire force. Therefore, readily available signal, i.e., a_x, was used to compare the estimated braking force with measured braking force. That is, the computed sum of the braking forces from the wheel dynamics of (1) is compared with the product of the M_v and a_x.

In addition, some tests on the dry asphalt demonstrated that the model uncertainty compensation degraded the estimation results because the amount of model uncertainty was very small compared with the experiments on the low mu surface. As mentioned, the proposed estimator is most effective when the brake pad surface is wet due to the driving or weather conditions. In this test, pad friction coefficient was not wet and does not allow changes in pad surface conditions. That is, the pad friction coefficient was more robust to other external environment factors such as temperature and pad wear level but sensitive to the level of wetness on the pad surface.

Therefore, these aspects should be considered when the proposed estimator is implemented in the electronic control unit (ECU). For example, the estimator can be suspended when the deceleration is over a defined threshold because the threshold indicates that the vehicle is traveling on a surface mu, which is larger than the threshold.

Next, in order to confirm the robustness of algorithm against the surface transition, the vehicle was driven quickly onto a different road surface as depicted in Fig. 14. The surface transition from the dry asphalt to the basalt surface occurred at $t = 9$ s. At the moment of transition, the front wheel speeds decreased slightly due to the reduced road surface friction coefficient. That is, front wheel slip ratio increased after the surface transition as shown in Fig. 14(d). However, the rear wheel attempted to maintain its speed, although a surface transition had occurred. As a result, only the front brake torque varied due to the model uncertainty compensation, as depicted in Fig. 14(f).

In this experiment, the test driver attempted to maintain the deceleration about 0.45 g by adjusting brake pedal travel regardless of the road friction transition. Due to this maneuver, no significant variation of the normalized forces was observed at each wheel. Instead, the front wheel slip ratio increased after the road surface transition, which provided nearly the same braking force as that of the dry asphalt.

In addition, there was insufficient time to change the pad surface condition in this experiment. That is, the time allowed to change the characteristics of the brake pad surface condition was approximately 3 s after the surface transition occurred, as depicted in Fig. 14(a). Considering road surface transition in the real world, this was reasonable. Because the surface of the brake pad stuck to the disk wheel, the road surface condition was changed but the friction coefficient of the pad surface did not change immediately. Moreover, since the brake pads are protected by the outer structure of the wheel, it is difficult to wet the pads with insufficient water on the road.

Therefore, the model uncertainty compensation was not dependent on the pad surface condition in this experiment, but it was only influenced by the current normalized forces at each wheel. However, if the vehicle continued to decelerate on the road where there was sufficient water, the pad friction coefficient would have decreased significantly.

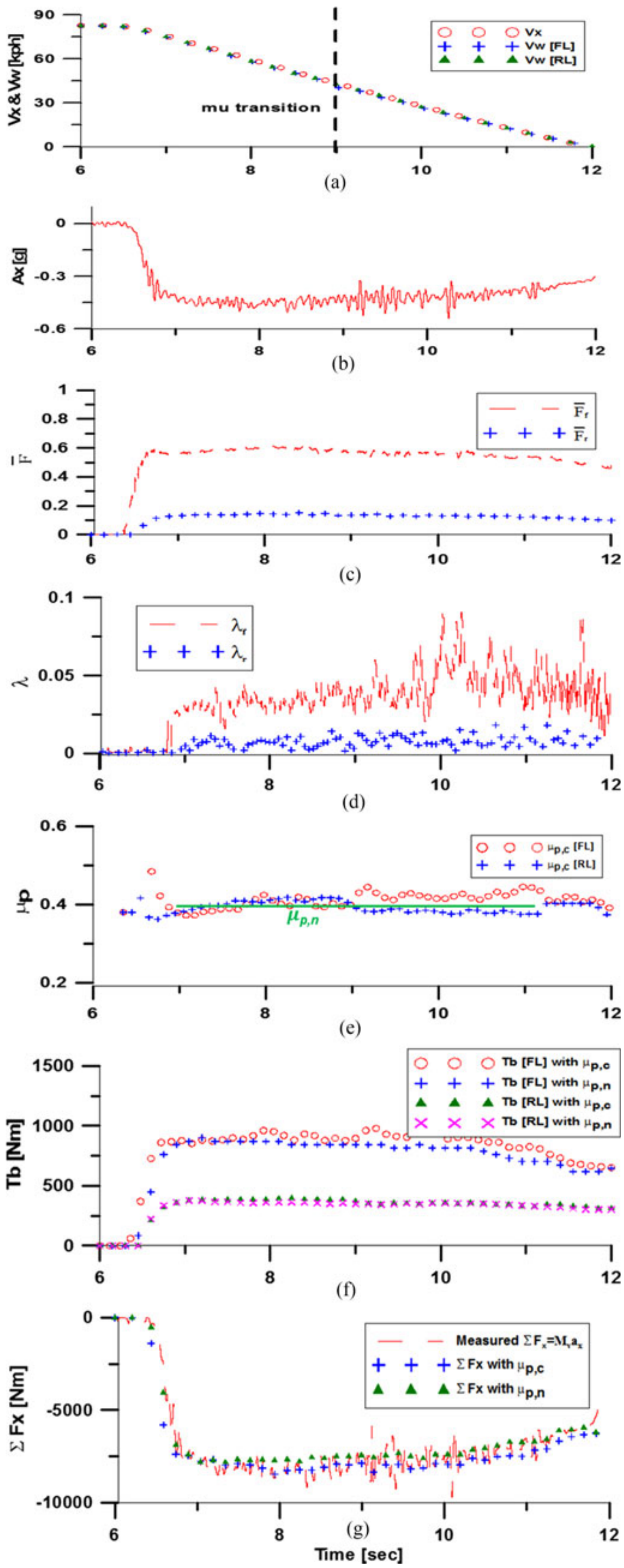

Fig. 14. Algorithm verification on a surface transition $\mu_{\max} \approx 1.0 \rightarrow \mu_{\max} \approx 0.6$.

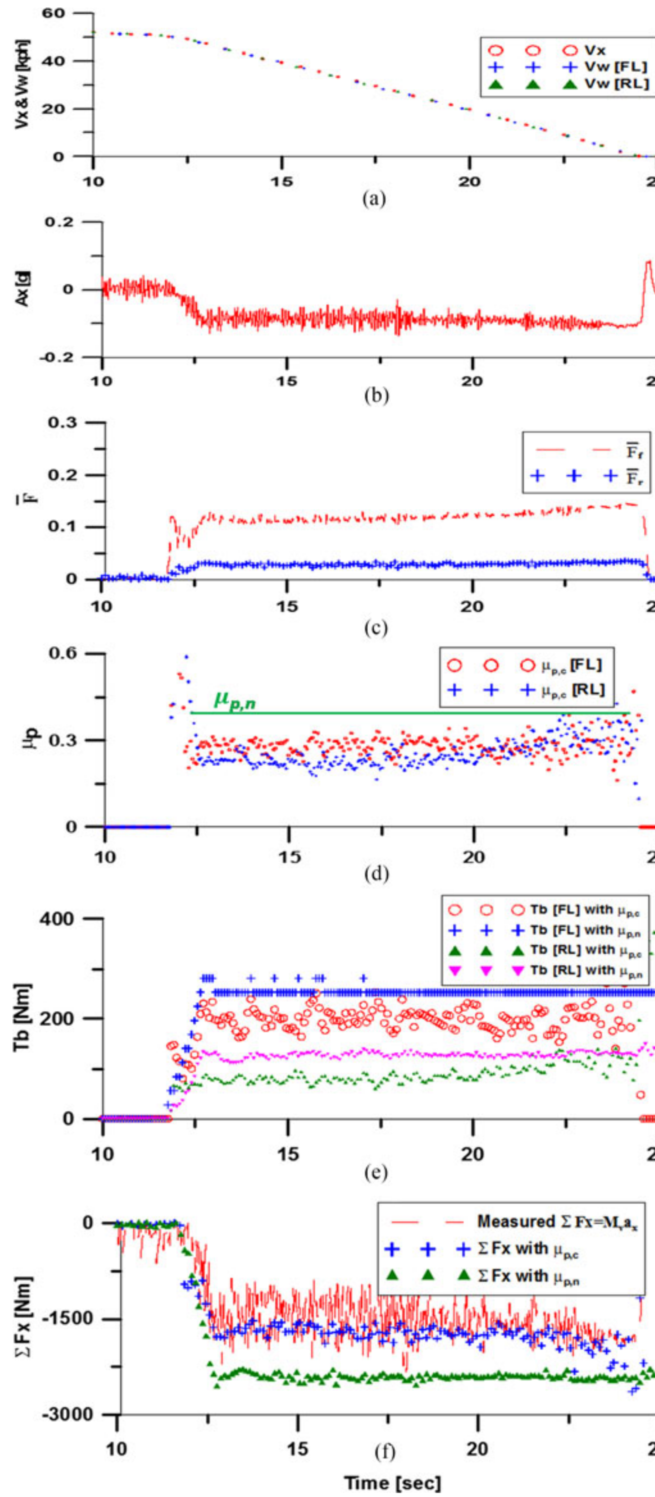

Fig. 15. Algorithm verification on a wet tile road surface with $\mu_{\max} \approx 0.2$.

To summarize the results of Fig. 14, the vehicle decelerated as if it was traveling on a homogeneous surface, and only the front wheel slip was varied to provide the required braking force. Also, no significant variation of normalized forces was observed due to the unwet brake pad and driver's maneuver.

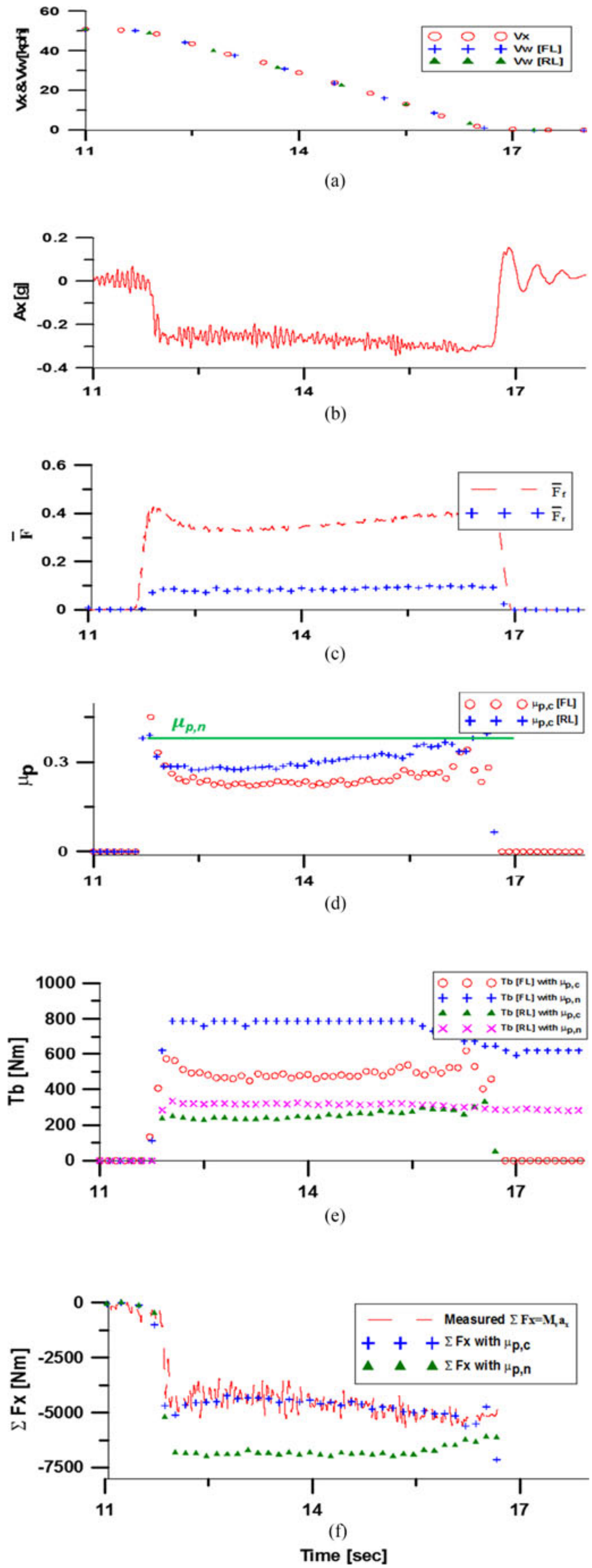

Fig. 16. Algorithm verification on a Basalt road surface with $\mu_{\max} \approx 0.45$.

Compared with previous experiments, core contribution of this paper is verified at the third experiment on the wet tile surface that provides a very low mu of approximately $\mu_{max} \approx 0.2$. Before starting the verification, the test vehicle stayed sufficient time on a wet road surface by the sprinkler system to change the pad surface condition. Fig. 15 presents the estimation performance of the developed algorithm implemented in the test vehicle. The test maneuvers were depicted in Fig. 15(a) and (b), and constant deceleration is maintained until the vehicle stopped. Fig. 15(d) described the compensated pad friction coefficients that were assumed in order to include all model uncertainties. The compensated pad friction coefficients using the proposed method were significantly lower than the nominal friction coefficients, and it improved the brake torque estimation performance as depicted in Fig. 15(e). With the $\mu_{p,n}$, the calculated brake torque could not provide practical information; however, the estimation results after the model compensation scheme was applied, provided more reasonable brake torques.

The braking force could be also verified through analyzing the sum of the measured longitudinal braking force.

As described in Fig. 15(f), estimated braking force with $\mu_{p,c}$ was significantly closer to the measured braking force that was calculated through multiplying the longitudinal deceleration and gross vehicle weight. However, it was clear that the estimated braking force when $\mu_{p,n}$ was used could not reflect the practical aspects due to the variations in the external driving environments.

Similar to the third experiment, the test vehicle was driven on a flat road surface that provides a medium surface friction with $\mu_{max} \approx 0.45$. Fig. 16 presents the test results implemented using the same test vehicle as the previous experiments. The proposed observer effectively reflected the variation in the driving environment, even with changes in the test driving course. Furthermore, it could be seen in Fig. 16(d) that the wheel dynamic model was compensated through reducing the pad friction coefficient using the adaptation scheme.

In summary, it can be said that these experimental validations demonstrated the effectiveness of proposed method when the vehicle traveled on the low mu surfaces with wet brake pad surface like Figs. 15 and 16.

VI. Conclusion

A new strategy to estimate the individual brake torque was developed and investigated with simulations and experiments. The key contribution that distinguishes this method from the previously reported methods is that it considers practical concerns when the brake force is applied on wet road surfaces. Largely influenced by the driving or weather conditions, the amount of brake torque is by the altered brake pad friction coefficient. Therefore, it was assumed that pad friction coefficients are the only uncertainties of the wheel dynamics model and it was compensated using the brake force distribution characteristic and the adaptive scheme. The simulation and experiment results using the proposed algorithm demonstrate that the proposed method can be implemented in passenger vehicles without additional sensors or modification of the control system. Therefore, improved active chassis control is anticipated. However, some minor issues such as threshold setting for preventing performance degradation require further investigation.

REFERENCES

[1] H. Her, Y. Koh, E. Joa, K. Yi, and K. Kim, "An integrated control of differential braking, front/rear traction, and active roll moment for limit handling performance," *IEEE Trans. Veh. Technol.*, vol. 65, no. 6, pp. 4288–4300, Jun. 2016.

[2] X. Ran, X. Zhao, J. Chen, and C. Yang, "Novel coordinated algorithm for traction control system on split friction and slope road," *Int. J. Automotive Technol.*, vol. 17, pp. 817–827, 2016.

[3] L. Xiong, G. Teng, Z. Yu, W. Zhang, and Y. Feng, "Novel stability control strategy for distributed drive electric vehicle based on driver operation intention," *Int. J. Automotive Technol.*, vol. 17, pp. 651–663, 2016.

[4] H. Zhu, L. Li, M. Jin, H. Li, and J. Song, "Real-time yaw rate prediction based on a non-linear model and feedback compensation for vehicle dynamics control," *Proc. Inst. Mech. Eng., D, J. Automobile Eng.*, vol. 227, pp. 1431–1445, 2013.

[5] A. Rezaeian *et al.*, "Novel tire force estimation strategy for real-time implementation on vehicle applications," *IEEE Trans. Veh. Technol.*, vol. 64, no. 6, pp. 2231–2241, Jun. 2015.

[6] T. Hsiao, "Robust wheel torque control for traction/braking force tracking under combined longitudinal and lateral motion," *IEEE Trans. Intell. Transp. Syst.*, vol. 16, no. 3, pp. 1335–1347, Jun. 2015.

[7] S. B. Choi, "Antilock brake system with a continuous wheel slip control to maximize the braking performance and the ride quality," *IEEE Trans. Control Syst. Technol.*, vol. 16, no. 5, pp. 996–1003, Sep. 2008.

[8] N. El-Tayeb and K. Liew, "On the dry and wet sliding performance of potentially new frictional brake pad materials for automotive industry," *Wear*, vol. 266, pp. 275–287, 2009.

[9] W. Cho, J. Yoon, S. Yim, B. Koo, and K. Yi, "Estimation of tire forces for application to vehicle stability control," *IEEE Trans. Veh. Technol.*, vol. 59, no. 2, pp. 638–649, Feb. 2010.

[10] H. Hamann, J. K. Hedrick, S. Rhode, and F. Gauterin, "Tire force estimation for a passenger vehicle with the unscented Kalman filter," in *Proc. 2014 IEEE Intell. Veh. Symp.*, 2014, pp. 814–819.

[11] M. Choi, J. J. Oh, and S. B. Choi, "Linearized recursive least squares methods for real-time identification of tire–road friction coefficient," *IEEE Trans. Veh. Technol.*, vol. 62, no. 7, pp. 2906–2918, Sep. 2013.

[12] R. Rajamani, G. Phanomchoeng, D. Piyabongkarn, and J. Y. Lew, "Algorithms for real-time estimation of individual wheel tire-road friction coefficients," *IEEE/ASME Trans. Mechatronics*, vol. 17, no. 6, pp. 1183–1195, Dec. 2012.

[13] J. Wang, L. Alexander, and R. Rajamani, "Friction estimation on highway vehicles using longitudinal measurements," *J. Dyn. Syst. Meas. Control*, vol. 126, pp. 265–275, 2004.

[14] L. Li, K. Yang, G. Jia, X. Ran, J. Song, and Z.-Q. Han, "Comprehensive tire–road friction coefficient estimation based on signal fusion method under complex maneuvering operations," *Mech. Syst. Signal Process.*, vol. 56, pp. 259–276, 2015.

[15] K. S. Han, E. Lee, M. Choi, and S. B. Choi, "Adaptive scheme for the real-time estimation of tire-road friction coefficient and vehicle velocity," *IEEE/ASME Trans. Mechatronics*, doi:10.1109/TMECH.2017.2704606.

[16] C. Lee, K. Hedrick, and K. Yi, "Real-time slip-based estimation of maximum tire-road friction coefficient," *IEEE/ASME Trans. Mechatronics*, vol. 9, no. 2, pp. 454–458, Jun. 2004.

[17] C. M. Martínez, E. Velenis, D. Tavernini, B. Gao, and M. Wellers, "Modelling and estimation of friction brake torque for a brake by wire system," in *Proc. IEEE Int. Elect. Veh. Conf.*, 2014, pp. 1–7.

[18] J. J. Oh and S. B. Choi, "Vehicle velocity observer design using 6-d imu and multiple-observer approach," *IEEE Trans. Intell. Transp. Syst.*, vol. 13, no. 4, pp. 1865–1879, Dec. 2012.

[19] K. A. Morris, *Introduction to Feedback Control*. Orlando, FL, USA: Academic, 2000.

[20] M. Ehsani, Y. Gao, and A. Emadi, *Modern Electric, Hybrid electric, and Fuel Cell Vehicles: Fundamentals, Theory, and Design*. Boca Raton, FL, USA: CRC press, 2009.

[21] P. A. Ioannou and J. Sun, *Robust Adaptive Control*. Upper Saddle River, NJ, USA: Courier Corporation, 2012.

[22] H. Pacejka, *Tire and Vehicle Dynamics*. New York, NY, USA: Elsevier, 2005.

[23] K. Han, Y. Hwang, E. Lee, and S. Choi, "Robust estimation of maximum tire-road friction coefficient considering road surface irregularity," *Int. J. Automotive Technol.*, vol. 17, pp. 415–425, 2016.

[24] H. K. Khalil and J. Grizzle, *Nonlinear Systems*, vol. 3. Englewood Cliffs, NJ, USA: Prentice-Hall 1996.

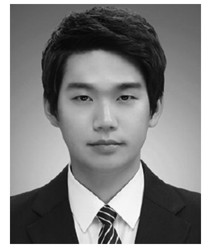

Kyoungseok Han received the Bachelor's degree in civil engineering (minor in mechanical engineering) from Hanyang University, Seoul, Korea in 2013 and the M.S. degree in mechanical engineering from the Korea Advanced Institute of Science and Technology (KAIST), Daejeon, Korea, where he is currently working toward the Ph.D. degree in mechanical engineering. His current research interests include vehicle dynamics and control, vehicle state estimation, and control theory.

Seibum B. Choi (M'09) received the B.S. degree in mechanical engineering from Seoul National University, Seoul, Korea, in 1985, the M.S. degree in mechanical engineering from the Korea Advanced Institute of Science and Technology (KAIST), Daejeon, Korea, in 1987, and the Ph.D. degree in control from the University of California, Berkeley, CA, USA, in 1993. From 1993 to 1997, he was involved in the development of automated vehicle control systems at the Institute of Transportation Studies, University of California. During 2006, he was with TRW, Warren, MI, USA, where he was involved in the development of advanced vehicle control systems. Since 2006, he has been with the faculty of the Mechanical Engineering Department, KAIST. His current research interests include fuel-saving technology, vehicle dynamics and control, and active safety systems.

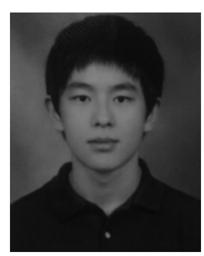

Jonghyup Lee received the Bachelor's and M.S. degrees in mechanical engineering from the Korea Advanced Institute of Science and Technology (KAIST), Daejeon, Korea, where he is currently working toward the Ph.D. degree in mechanical engineering. His current research interests include tire modeling and vehicle state estimation.

Dongyoon Hyun received the B.S. and M.S. degrees in agricultural mechanical engineering from Seoul National University, Seoul, Korea. After graduation, he worked five years for the Agency for Defense Development in Korea where he was involved in research and development of army vehicles. He began his graduate studies again in 1996 and received the M.S. and Ph.D. degrees in Mechanical Engineering from Texas A&M University in 1997 and 2001, respectively. Since 2003, he has worked as a Senior Research Engineer at Hyundai-Kia R&D Center, and has been responsible for developing advanced chassis control systems.

Jounghee Lee received the Bachelor's degree in mechanical engineering from Yonsei University, Seoul, Korea, in 2009. He is currently with the Chassis System Control Development Team, Hyundai Motor Company, Hwaseong, Korea.

His research interests include integrated control systems in chassis and intelligent vehicle safety systems.